Chemical Engineering Journal 151 (2009) 275–285

Contents lists available at ScienceDirect

Chemical Engineering Journal

journal homepage: www.elsevier.com/locate/cej

Treatment of leather plant effluent using NF followed by RO and permeate flux prediction using artificial neural network

M.K. Purkait[a,*], V. Dinesh Kumar[b], Damodar Maity[c]

[a] Department of Chemical Engineering, Indian Institute of Technology Guwahati, Guwahati 781039, India
[b] Department of Civil Engineering, Indian Institute of Technology Guwahati, Guwahati 781039, India
[c] Department of Civil Engineering, Indian Institute of Technology Kharagpur, Kharagpur 721302, India

ARTICLE INFO

Article history:
Received 28 June 2007
Received in revised form 24 February 2009
Accepted 3 March 2009

Keywords:
Permeate flux
Leather effluent
Artificial neural networks
Back-propagation algorithm
Membrane filtration

ABSTRACT

This paper presents experimental data and modeling for membrane-based treatment of leather plant effluent. The effluent coming out from the various upstream steps of leather plant are combined and pressure driven membrane processes like nanofiltration (NF) and reverse osmosis (RO) are undertaken after a pretreatment consisting of gravity settling and coagulation followed by cloth filtration. Performances of two NF membranes (200 and 400 molecular weight cut offs (MWCO)) are evaluated. Experiments are conducted using an unstirred batch cell. It is observed that a combined operation of NF using 400 MWCO membrane followed by RO operation is better option compared to a single operation of NF with 200 MWCO (membrane). After selection of proper NF membrane from batch experimental data, the entire membrane separation scheme is validated by conducting experiments using a cross flow cell. A detailed parametric study for cross flow experiment is investigated and the suitable operating trans-membrane pressure and the cross flow rates are found out (experimentally) in both NF and RO. The experimental flux data are correlated and analyzed using artificial neural network (ANN). A multi-layered feed-forward network with back-propagation algorithm is used for training of ANN models. Two artificial neural network models with input, output and hidden layer(s) are used to predict the flux data for both the batch and cross flow run. A good agreement has been observed using the ANN model with the experimental flux data with a deviation not more than 1% for most of the cases considered. The BOD and COD values of the finally treated effluent are well within the permissible limits.

1. Introduction

Around 70,000 tones of hides and skins are processed each year in India, releasing ~75,000 m^3/day of the waste water [1]. The main ingredients are sodium chloride, sodium sulfide, lime, chromium, protein, fats, etc. [2]. Small-scale tanneries dispose the effluents from the "beam house" through a common header directly to the sewage/river stream. In search of "cleaner technology", the membrane-based processes are successfully used for the treatment of leather plant effluent. Cassano et al. [3] presented a detailed survey of the applications of the membrane-based processes, e.g., microfiltration (MF), ultrafiltration (UF), nanofiltration (NF) and reverse osmosis (RO) on various effluent streams of the "beam house". Application of UF to the effluent from the liming [4], degreasing [5,6] have been reported. The use of UF and RO to treat the soaking, deliming/bating and pickling effluents are proposed [3]. The removal and reuse of dyes from dyeing unit is also reported [7]. Treatment of the chromium rich tanning effluents using UF and NF is mostly studied [8–12] for the recovery and reuse of tanning chemicals.

Although, the membrane-based processes are attractive, the inherent limitation of these processes is the decline of flux. The throughput of these processes decrease with the time of the operation because of membrane fouling and concentration polarization (i.e., deposition/increase of concentration of solutes over the membrane surface). Therefore, in order to scale up the systems, the flux decline mechanism should properly be understood. It is well established that the dead end filtration experiments are the most suitable option for better fundamental understanding of flux decline mechanism. Several reports are available for the treatment of leather plant effluent using membrane-based processes [3,5,6]. Various flux decline mechanisms are proposed in the literature, e.g., osmotic pressure governed flux decline [13,14], gel or cake layer controlled flux decline [15,16], various steps for blocking the membrane pores, like, complete pore blocking, standard pore blocking, intermediate pore blocking, etc. [17,18]. Among these, one or more steps may be involved simultaneously to cause the flux decline. In most of the studies, it is proposed that early stage of flux decline is due to some

* Corresponding author. Tel.: +91 361 2582262; fax: +91 361 2582291.
E-mail address: mihir@iitg.ernet.in (M.K. Purkait).

1385-8947/$ – see front matter © 2009 Elsevier B.V. All rights reserved.
doi:10.1016/j.cej.2009.03.023

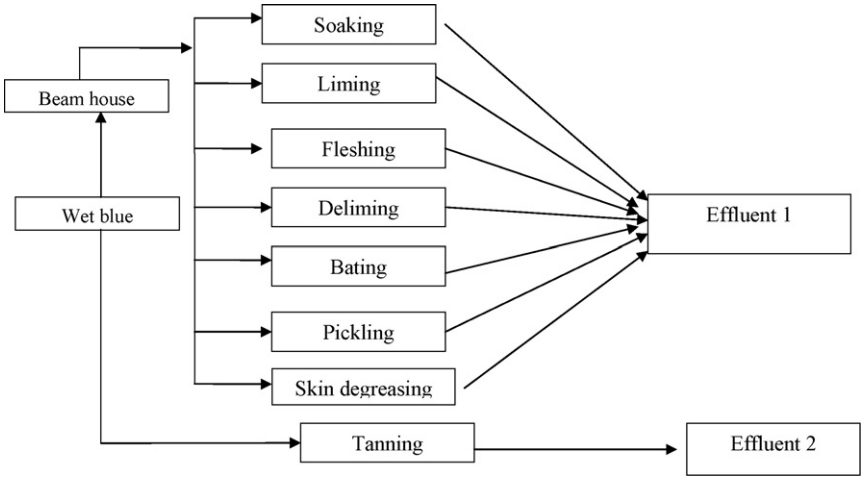

Fig. 1. Generation of effluent from various processing stages of a typical leather plant.

kind of pore blocking, followed by cake filtration for long term flux decline [19–25]. Modeling studies of flux decline during MF and UF of protein solution using these mechanisms are available in literature [19–22]. Similar type of flux decline mechanisms are studied for MF of apple juice [23], beer [24], surimi wash water [25], waste water [26], humic acid [27] as well as for UF of surfactant micelles [28], cheese whey [29], natural organic matters [22], etc. Although several reports are available for the treatment of leather plant effluent using membrane-based processes [6–8], the identification of flux decline mechanism as well as its quantification studies are rare.

However, the effects of process conditions on membrane performance (permeate flux and rejection) and their dynamic behaviors are usually non-linear in nature. Therefore, the predictions of the conventional models are not always satisfactory. Thus there is a need for alternative methods such as artificial neural network (ANN) approach. A neural network can be used to simulate the non-linear input/output dynamics of a process based on a time history of process data [30]. An ANN is composed of many single elements called neurons. These neurons are connected to each other in different ways and therefore formed different types of ANN. The most popular ANN is the multi-layer feed-forward neural network where the neurons are arranged into three layers: input layer, hidden layer, and output layer [31]. Feed-forward neural network usually has one or more hidden layers, which enable the network to deal with the non-linear and complex correlation [32,33].

Application of the membrane-based processes to treat each of the "beam house" effluent separately is probably a costly proposition. In this work, a scheme is proposed to treat the leather plant effluent using a two-step pressure driven membrane separation processes involving NF and RO. Detailed parametric study is carried out using batch and continuous cross flow system. Neural network models have been used to describe the permeate flux profiles during NF and RO of leather plant effluent dynamically for both batch and cross flow run. It aims to predict the permeate flux at different operating condition with processing time. A multi-layer feed-forward network structure with input, output and hidden layer(s) is used in this study. The back-propagation algorithm is utilized in training of ANN models. The modeling results showed that there is an agreement between the experimental data and predicted values, with mean absolute errors less than 1% of the experimental data.

2. Proposed scheme

2.1. Effluents

In a leather plant, two major effluent streams are generated from the "wet blue" step of the processing. The leather from "wet blue" goes to the "beam house" for several chemical consuming steps in series; e.g., soaking, liming, defleshing, bating, pickling, etc. and the tanning step which generates the chromium rich effluent as shown in Fig. 1. Membrane-based separation of the mixture all the effluent may be useful but problem arises with the retentate, which contains concentrated toxic chromium ion. To overcome this problem and also to use retentate sludge as manure and to reuse chromium for further use, overall leather plant effluent is divided into two parts; namely, (a) the common effluent from soaking to skin degreasing (including seven steps), is termed as effluent 1 which does not contain chromium; (b) the effluent from the tanning step which contains toxic chromium metal ions, termed as effluent 2.

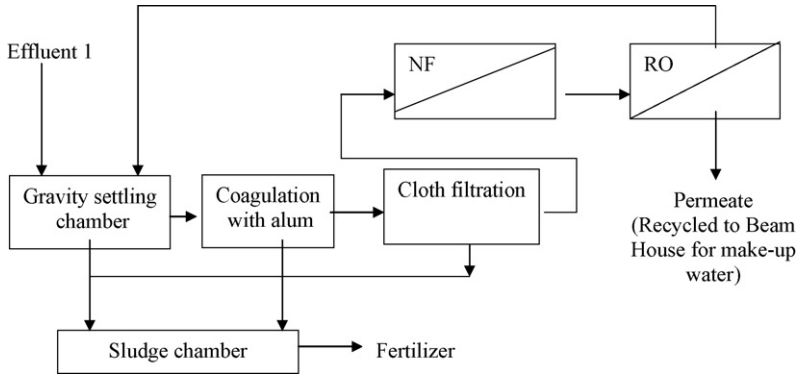

Fig. 2. Proposed scheme for the treatment of effluent 1.

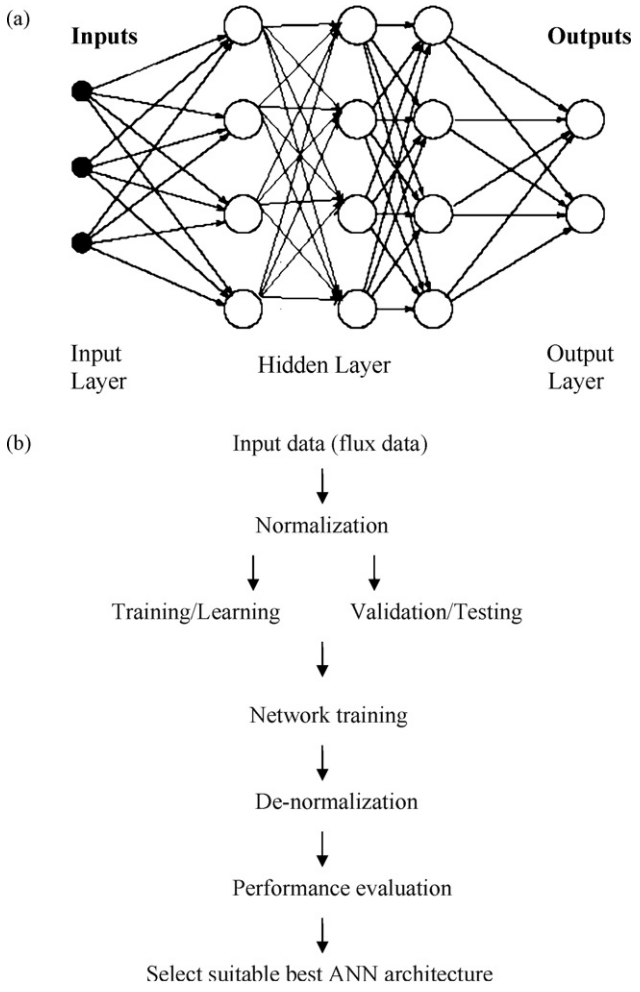

Fig. 3. (a) Structure of feed-forwarded network with three hidden layer and one output layer. (b) Methodology for ANN architecture.

Treatment of effluent 2 is already discussed in the literature [8–12]. In this work, treatment of effluent 1 is addressed. Effluent 1 (devoid of chromium) contains lots of organic and inorganic chemicals. It is proposed that the effluent 1 is first subjected to gravity settling. The supernatant is then subjected to coagulation by alum. This process generates mostly an organic sludge. The supernatant of this coagulation step is then filtered by a fine filter cloth. The sludge produced in gravity settling, coagulation and the cloth filtration is stored in a common chamber which may be used as fertilizer. The clarified effluent is then subjected to a two step membrane-based separation processes; namely, NF followed by RO using both batch and cross flow cell. The performance criteria of these membrane processes are evaluated in terms of COD, BOD and the permeate flux of the treated effluent. The permeate flux indicates the throughput (quantity) of the product; whereas other properties indicate the quality of the product. The validity of the above scheme is tested in a batch cell due to two reasons. First, the conduction of the experimental runs in the batch cell is easy and second, the batch cell experiments are at the worst possible conditions. As the time of the experiment progresses, the bulk concentration increases and the membrane fouling and concentration polarization becomes severe leading to worse permeate quality. In other words, if an experimental scheme is successful in a batch cell, in terms of the permeate quality and the flux, then that scheme must be successful in a continuous steady mode; either in a stirred or in a cross mode. It is envisaged that the retentate of both the membrane processes can be recycled to the gravity settling chamber for further processing and the final permeate of RO can be recycled back to the "beam house" for make up water and chemicals. The schematic of the treatment of the effluent 1 is shown in Fig. 2. Once the scheme for the membrane separation process is validated in the batch cell, cross flow experiments are conducted in detail.

Table 1
Characterization of leather plant effluent 1.

Effluent characteristic	Value
COD (mg/L)	4335
BOD (mg/L)	1800
PH	3.4
Conductivity (mS)	138
TDS (g/L)	92
TS (g/L)	116
Turbidity (NTU)	157

2.2. Neural network

An artificial neural network is a framework consisting of many number of neuron like processing units. Each neuron is simulated by the sum of the incoming weighted signals and transmits the activated response to the other connected neuron units. Such a network represents an efficient and parallel computational entity and will reflect the level of simulations by different input signals. The dynamic weights which connected neuron of different layer continuously modified during the process of learning. Multi-layer feed-forward neural network with back propagation algorithm is used to train the models frequently. Neurons are arranged in three layers: input layer, hidden layer, and output layer [31] as shown in Fig. 3a.

Back-propagation is a special technique used for implementing gradient-descent in weight space for a multi-layer feed-forward network, in which the network weights are moved along the negative of the gradient of the performance function. Back propagation refers to the manner in which the gradient is computed for non-linear multi-layered networks. Neural networks with single and multiple hidden layers containing a sufficient number of neurons map accurately the input and the output of the network. Activation function and transfer function are selected according to the problem. Network inputs and outputs are problem specific. Input for the network is normalized, and this normalized input data is divided for training and validation randomly. ANN model with different experimental conditions is tested for training and validation data. Over training of network has to be avoided as it remembers the input output mapping exactly rather than training network properly. Weights are adjusted till acceptable mean square error is achieved by training the network. Fig. 3a shows the basic structure of multi-layer feed-forward neural network with back propagation algorithm technique. Methodology for developing ANN architecture has been explained in Fig. 3b.

3. Experimental

3.1. Effluent

Effluent 1 is collected from M/s Alison Tannery, Kolkata, India. It is collected from the main drain, which contains all the effluent from "wet blue" process except the chrome tanning. The characterization of the effluent has been carried out and is presented in Table 1.

3.2. Chemicals used

Potassium alum is used for the coagulation and is procured from the local market. All the chemicals, required for the determination

of chemical oxygen demand (COD) and biological oxygen demand (BOD), are procured from Loba Chemie India and are used without further treatment.

3.3. Membrane

Organic polyamide membranes of molecular weight cut off (MWCO) of 200 and 400 are used for nanofiltration (NF). Thin film composite polyamide membrane is used for reverse osmosis (RO). To avoid the excess solid load over RO membrane, NF is used first. All the membranes are procured from M/s, Genesis Membrane Sepratech Pvt. Ltd., Mumbai, India. The permeabilities of the membrane are determined using distilled water and are estimated to be 3.25×10^{-11} m/Pa s for 400 MWCO, 2.88×10^{-11} m/Pa s for 200 MWCO and 7.52×10^{-12} m/Pa s for the RO membrane. The range of operating pressure for NF membrane is 414–966 kPa and that of for RO membrane is 828–1380 kPa.

3.4. Membrane filtration cells

3.4.1. Batch cell

The unstirred batch experiments are conducted in a 150-mL filtration cell made of stainless steel. Inside the cell, a flat circular membrane is placed over a metallic support. The membrane diameter is 4.5×10^{-2} m and the effective area of the membrane is 15.9×10^{-4} m^2. The permeating solution, from the bottom of the cell, is collected. The cell is pressurized using a nitrogen cylinder. The schematic of batch experimental set up is presented elsewhere [34].

3.4.2. Cross flow cell

The clarified effluent is pumped by a high pressure reciprocating pump from the stainless steel feed tank to the cross flow cell with a rectangular channel. The effective length of the membrane is 37.3×10^{-2} m and width is 5.2×10^{-2} m. The channel height is determined by the thickness of the rectangular *Teflon* gasket and the channel height is found to be 3.44×10^{-3} m. The retentate stream is recycled back to the feed tank. The pressure and the cross flow rate inside the membrane channel are independently set by operating the valves in the bypass line and that at the outlet of the membrane cell. Permeate samples are collected from the bottom of the cell and are analyzed. The schematic of cross flow experimental set up is presented elsewhere [35].

3.5. Operating conditions

In the batch cell, the operating variable is the transmembrane pressure only. The operating pressures are 414, 552 and 828 kPa for NF experiments. For RO, operating pressures are 828, 1104 and 1242 kPa. In the cross flow cell, the operating variables are the transmembrane pressure and the cross flow velocity. The operating pressures for NF and RO are the same as those in the batch cell. The cross flow rates are 30, 75 and 120 L/h. For RO runs, feed is generated by collecting the permeating solution through a NF membrane of 400 MWCO at 828 kPa.

3.6. Procedure

3.6.1. Pretreatment

Effluent 1 is kept in five numbers of 500 mL capacity containers. Alum is added to each of these at the concentration of 0.2, 0.5, 1, 2 and 3 g/L in order to obtain the optimum dose of the coagulant. The typical coagulation time is found to be 30 min. Once the optimum coagulant dose is obtained, the supernatant of the gravity settled liquor is treated with the optimum alum dose. The gravity settlement is carried out in a 10-L container for 2 days. After coagulation, the sludge settled at the bottom and the supernatant is siphoned out. The sludge of the gravity settling and the coagulation are mixed up and stored for the use as a fertilizer. A fine nylon filter cloth is then used for further clarification of the collected supernatant. The clarified liquor is then treated by the membrane separation processes.

3.6.2. Nanofiltration

In the membrane-based experiments, each membrane is first compacted with distilled water using a higher pressure of the maximum operating pressure. The membrane permeability is estimated from the permeate flux versus pressure data, using distilled water. After that, the cell is charged with the clarified effluent. The duration of the batch cell experiments are of 2 h and those for the cross flow experiments are of 1 h. The permeating solution is collected on a digital balance on a cumulative volume basis. From the slope of the cumulative volume versus time curve, the permeate flux is calculated. The permeate samples are collected in regular intervals for analysis.

3.7. Analysis

The conductivity, total dissolve solids (TDS), turbidity and pH of all samples (feed, permeate and retentate streams at each operating conditions) are measured at room temperature using a deluxe water and soil analysis kit, model no 191E, manufactured by Toshniwal Instruments Ltd, India. Total solids (TS) of all the samples are measured by taking a known volume of sample in a petri dish and keeping in an oven maintained at $105 \pm 2\,^{\circ}$C; till complete drying of the sample. COD and BOD are determined using standard techniques [36].

3.8. ANN procedure

In this section, detailed procedure for the approach of ANN network is produced. Normalization of data, ANN architecture development, training of neural network and optimal ANN configuration selection has been discussed in this section. Network stopping criteria have been elaborated by Jindal and Chauhan [37]. As the number of neurons or number of iterations increase, error decreases and network performance improves for training and validation data. Validation error starts to increase, as the number of iterations increase, while training error continues to decrease.

3.8.1. Normalization of data

Network inputs and output vectors are scaled to a desired numerical range for a particular transformation function, which is to the output range of transfer function. Numerical overflows can be avoided by normalization of input data for very large or small weights. Log-sigmoid function is used for training of the network. Range of the function lies in between 0 and 1, so input and output data should be normalized to the range of transformation function used. The normalized variable X_{norm} can be represented as

$$X_{norm} = \left\{ \frac{(y - 0.1)(y_{max} - y_{min})}{(0.8)} \right\} + y_{max}; \quad (1)$$

where y is the output values, y_{max} and y_{min} are the maximum and minimum values of the output values. Input and output data are normalized to the range of 0–1. Normalized output values containing 1 produce more error after training. So values in between the range of 0 and 1 are used for training after normalization of the data.

3.8.2. ANN network architecture

The manner in which the neurons of a network are structured in various layers, and the inter-connection between neurons between

Table 2
Experimental conditions and number of data used for training and validation of ANN (batch cell experimental data).

Exp	MWCO	Pressure (kPa)	TDS	Training	Validation
1	200	414 552 828	13.7	57	15
2	400	414 552 828	13.7	57	15
3	RO	828 1104 1242	8.27 8.64 9.6	57	15
	Total			171	45

Table 3
Experimental conditions and number of data used for training and validation of ANN (cross flow experimental data).

Exp	MWCO	Flow rate	TMP (kPa)	TDS	Training	Validation
1	400	120	414 552 828	8.27 8.64 9.6	360	36
2	400	75	414 552 828	8.27 8.64 9.6	365	36
3	400	30	414 552 828	8.27 8.64 9.6	366	36
4	RO	120	828 1104 1242	8.27 8.64 9.6	161	24
5	RO	75	828 1104 1242	8.27 8.64 9.6	166	24
6	RO	30	828 1104 1242	8.24 8.64 9.6	180	24
	Total				1598	180

each layers are important in this network architecture design. In general there are three fundamental classes of network architectures, that single-layer, multi-layer, and recurrent feed-forward networks. Among these multi-layer feed-forward networks with proper activation function is used because of its accuracy to the experimental data after training. Multi-layer feed-forward network contains one or more hidden layers in the network. Similarly among various activation functions log sigmoid function is used for our training.

Number of hidden layers and number of neurons in hidden layer are problem specific and can be selected by trail and error method [38]. As there is no fixed method to take number of hidden layers and neurons for a given problem, network is trained for various hidden layers and number of neurons for the best results. Among these one hidden layer with a particular number of neurons with less error prediction are selected as the network architecture. Learning rate and momentum rate are another important factors for proper training of the network. Rate of change of connection weights during training indicates the learning rate. Learning rate selection is of critical importance, as in finding the local or global error. A large or small learning rate does not solve a particular solution. Hence network is trained for best results with varying learning and momentum rate by trial and error method.

3.8.3. Neural network training

Both the batch and cross flow data are used for training purpose. Training for batch data set (1st training data set) consists of four inputs: membrane molecular weight cut off, trans-membrane pressure, time and total dissolved solids (TDS). Cross flow training data set (2nd training data set) consists of five inputs; molecular weight cut off, trans-membrane pressure, time total dissolved solids (TDS) and cross flow rate. The output of the network is permeate flux obtained from the batch and cross flow data. First and second training contain 216 and 1778 experimental data and shown in Tables 2 and 3, respectively. Training network with proper architecture, learning rate, momentum factor and number of iterations produce proper solution to the network. Weights associated with each neuron are adjusted in order to produce the actual response. For each neuron trained response is compared with the original experimental data and is produced in graphical form.

The number of hidden layers and neurons within each layer can be varied according to the complexity of the problem data. In this study, a feed-forward neural network model with varying hidden layers and number of neurons in the network are used. As numbers of hidden layers are increased network error is increasing, so training has been carried out with single hidden layer with varying neurons in the layer. The number of neurons used for training is two to seven for first set and in second set hidden layers and number of neurons in hidden layer are changed.

For a given set of inputs to the network, output layer response is calculated for each neuron and compared with the corresponding desired experimental output response. The weights associated with the network are adjusted in such a way that errors in each neuron compared above are minimized. Error minimization process is achieved using gradient descent rule [39]. Network structure with associated error, learning rate, momentum factor and number of neurons are presented in subsequent section. The prediction of accuracy of the ANN models was compared using Mean square error (MSE) of the network. Starting with a large MSE value, the performance of the network is observed and depending upon the accuracy required MSE value is reduced and trained initially for network's convergence.

4. Results and discussion

This section is divided into four parts. In the first part, pretreatment data of effluent 1 is reported and discussed. Analysis of batch experimental data is done in the second part. Cross flow experimental data is presented and explained well in the third part. ANN is used to predict the flux data of both batch and cross flow run for NF and RO membrane. Comparison of the performance of exclusive NF and NF followed by RO is done in the last part.

Table 4
Characterization of the clarified effluent after different alum doses.

Alum dose (kg/m^3)	COD (mg/L)	BOD (mg/L)	Turbidity (NTU)	TS (kg/m^3)	TDS (g/L)	pH
0.2	2970	1350	72.5	16.0	14.3	6.8
0.5	2880	1200	65.0	14.0	13.0	6.9
1.0	2280	850	43.8	14.0	12.8	7.7
2.0	2282	854	40.1	13.5	12.1	8.3
3.0	2284	856	38.2	13.5	11.9	8.6

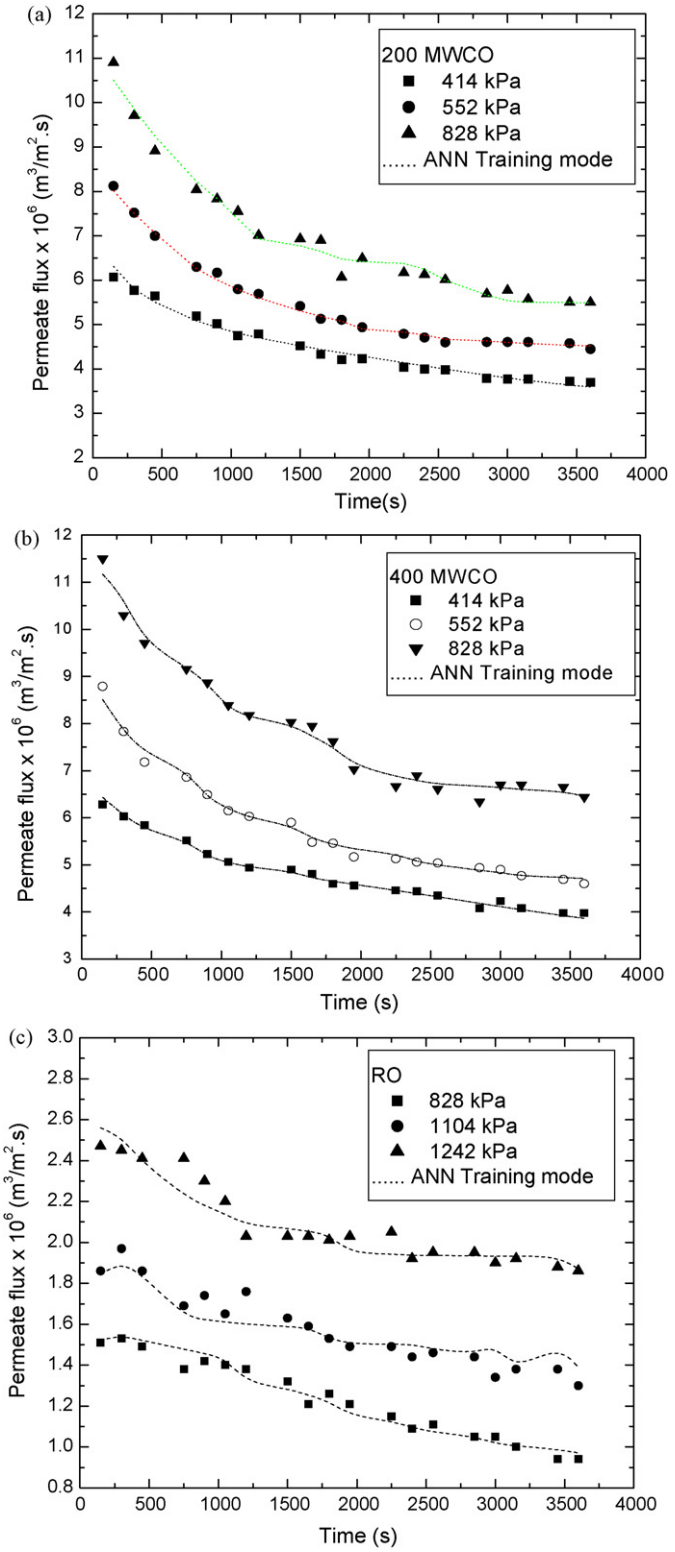

Fig. 4. (a) Permeate flux decline profiles along with ANN training mode data using 200 MWCO membrane in the batch cell under various operating pressures. (b) Permeate flux decline profiles along with ANN training mode data using 400 MWCO membrane in the batch cell under various operating pressures. (c) Permeate flux decline profiles along with ANN training mode data using RO membrane in the batch cell under various operating pressures.

Table 5
Properties of the permeating solution from RO at the end of 1 h of operation under batch mode.

Properties	Feed	828 kPa	1104 kPa	1242 kPa
pH	8.2	8.2	8.2	8.2
Conductivity (mS)	18.1	13.0	13.3	14.3
TDS (kg/m^3)	12.0	8.3	8.6	9.6
COD (kg/m^3)	378	72	108	128
BOD (kg/m^3)	154	30	45	54

4.1. Pretreatment

The supernatant of the pretreated effluent 1 is taken out and various properties, e.g., pH, conductivity, TDS, TS, turbidity, BOD and COD are measured. These properties of the alum treated effluent with the alum dose are tabulated in Table 4. It is clear from Table 4 that COD, BOD, turbidity, TS decrease sharply with the increase in alum dose up to 1.0 g/L; but, the decrease is marginal for higher dosages of alum. Therefore, 1.0 g/L is considered as the optimum alum dose. Further, pH at this level of alum concentration is almost neutral.

After establishing the optimum alum dose, the effect of gravity settling is investigated. It is observed that the gravity settlement of 2 days results in a decrease in COD from 4335 to 3768 mg/L. Therefore, the optimum alum dose is applied to the "gravity settled" solution and it results a COD and BOD of 864 and 388 mg/L, respectively; after the sludge separation. The amount of sludge generated is 102 g/L after drying, which can be used as a fertilizer. The other properties are found to be in the same range of those with optimally alum treated solution without the gravity settling. Therefore, the effluent 1 is first subjected to the gravity settling, followed by the alum treatment. The supernatant is then treated with the subsequent membrane filtration after a coarse filtration by a fine cloth.

4.2. Batch cell run

4.2.1. Nanofiltration

Two membranes, namely 200 and 400 MWCO are used separately to treat the clarified effluent 1. From the batch cell experiments, a better NF membrane is selected.

The permeate flux profiles for 200 and 400 MWCO membrane are shown in Fig. 4a and b, respectively, at different operating pressures. It may be observed from both the figures that there is a decline of the flux with time due to the membrane fouling and concentration polarization. There is 76% decline in flux (compared to the pure water flux) for 2 h of operation at 828 kPa pressure for 400 MWCO (membrane). For higher operating pressure, the flux values are more due to the increase in the available driving force. It may be observed that after 2 h of operation, the permeate flux increases from about 4.0×10^{-6} to 6.5×10^{-6} m^3/m^2 s when pressure rises from 414 to 828 kPa for 400 MWCO membrane. Compared to 400 MWCO membrane, the permeate flux values are always lower for 200 MWCO membranes as expected. For example, at 828 kPa pressure, the permeate flux for 400 MWCO membrane is

Table 6
ANN results for batch experimental data.

Sl. No.	Number of neurons	Mean square error ($\times 10^4$)	Number of iterations	Learning rate	Momentum rate
1	2	2.03	200	0.3	0.1
2	3	1.84	180	0.3	0.1
3	4	8.8	190	0.3	0.1
4	5	0.83	200	0.3	0.1
5	6	0.53	210	0.3	0.1
6	7	0.75	230	0.3	0.1

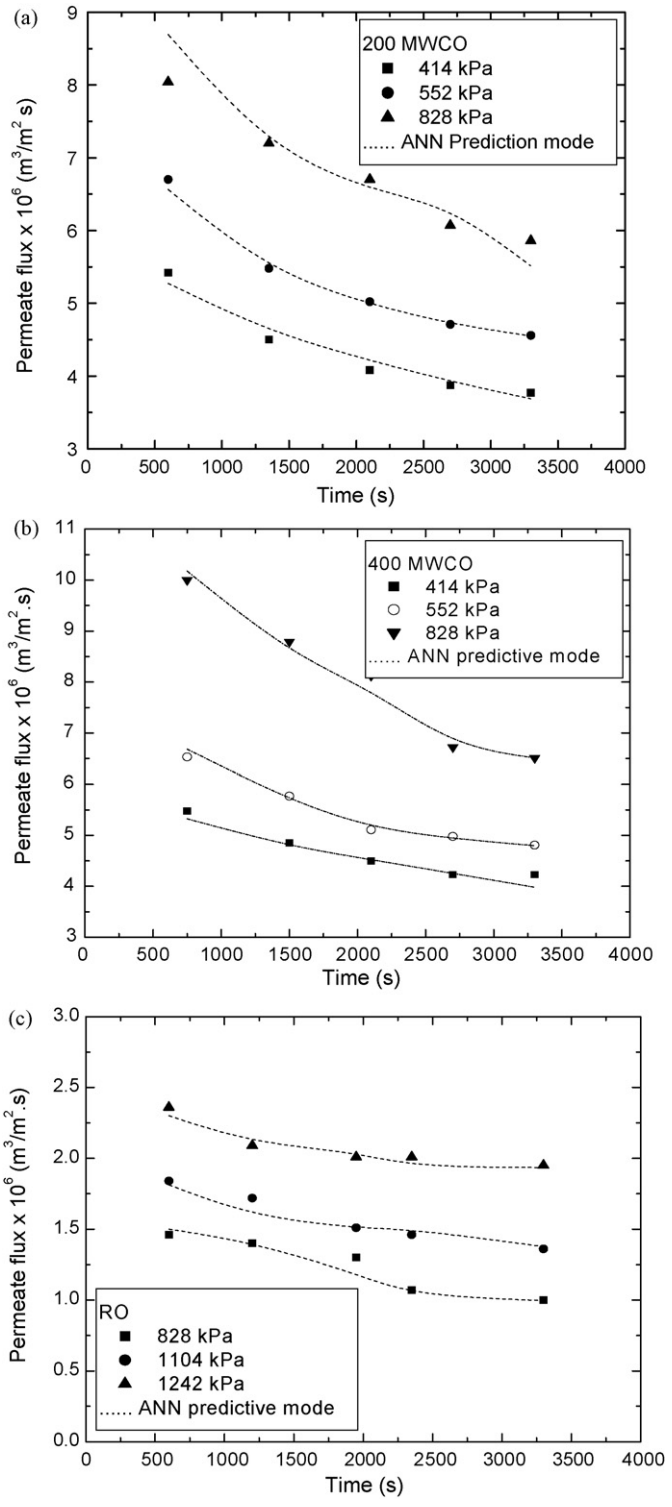

Fig. 5. (a) Permeate flux decline profiles along with ANN prediction using 200 MWCO membrane in the batch cell under various operating pressures. (b) Permeate flux decline profiles along with ANN prediction using 400 MWCO membrane in the batch cell under various operating pressures. (c) Permeate flux decline profiles along with ANN prediction using RO MWCO membrane in the batch cell under various operating pressures.

about 17% higher than that of 200 MWCO membrane at the end of the operation.

It is observed that the permeate conductivity and TDS increases marginally with time of operation. This is obvious as the filtration progresses, more inorganic solutes permeate through the membrane resulting in increasing in conductivity and TDS. Interestingly, at a fixed time, the conductivity and TDS is less for higher pressure. This may be due to the fact that the deposited layer of the organic solutes at the membrane surface gets more compact at higher pressure allowing less conductive solute to permeate. Although, it may be noted here, that the range of variation of conductivity and TDS is quite small. For example, conductivity varies between 14.2 and 17.2 mS and that for TDS is 9.5–12.5 g/L. At the end of 2 h of operation, the permeate conductivity and TDS are quite close to the feed values. For example, the feed conductivity is 18.4 mS; whereas, for 828 kPa pressure, permeate conductivity starts from 14.2 and after 2 h it is about 16 mS. For 414 kPa, it starts from 16 mS and reaches to about 17.4 mS after 2 h. Similar trend is observed for TDS. This indicates that the retention of the inorganic solutes by the membrane is quite low. The flux decline due to concentration polarization is mostly due to the presence of the organic solutes in the clarified effluent. Similar trends for TDS and conductivity are obtained for 200 MWCO membrane.

The most important permeate properties are COD and BOD. Since the COD and BOD of the permeating solution at the end of the batch experiments are measured. It is observed that both the BOD and COD increase with increase in pressure and the rate of increase slows down at higher pressure. For example, at 414 kPa pressure, the COD and BOD values are about 100 and 30 mg/L, which are within the environmental regulation (permissible limits for COD is 250 and that for BOD is 30 mg/L). For higher pressure these values are quite high. So, for NF using 400 MWCO (membrane), 414 kPa may be suitable operating pressure; but, this results in a low flux of about 3.5×10^{-6} m^3/m^2 s. If a higher operating pressure is selected, then BOD and COD go beyond the permissible limit. On the other hand for 200 MWCO (membrane), COD values are less than the permissible limit but BOD values are always greater than the permissible limits. Only for 414 kPa pressure, BOD is close to that limit. However, at 414 kPa pressure, the permeate flux for 200 MWCO membrane is about 8% lower than that of 400 MWCO membrane. Therefore, it is envisaged that NF by 400 MWCO at 828 kPa may be used to obtain the maximum permeate flux; and the permeating solution may then be subjected to low pressure reverse osmosis (RO) to bring down both the BOD and COD levels. This is discussed in the subsequent section.

4.2.2. NF followed by RO

The permeate flux decline of the RO is presented in Fig. 4c at the three pressures; namely, 828, 1104 and 1242 kPa. It may be noted that the flux decline is not as severe as that of NF, since the NF membrane retains most of the organic solutes. The flux decline shows the usual trend, i.e., the flux is more at higher pressure. At 1242 kPa pressure, the flux is about 1.8×10^{-6} m^3/m^2 s compared to 1.0×10^{-6} m^3/m^2 s at 828 kPa. The variation of other properties, e.g., pH, conductivity etc. are shown in Table 5 after 1 h of operation (half run). It shows that pH remains same for three pressures. Conductivity and TDS increase marginally with pressure but COD and BOD show definitely increasing trend with pressure. The final values of COD and BOD at the end of the experiments (after 2 h) are 160 mg/L and 68 mg/L, respectively, at 1242 kPa pressure. It may be noted here that the BOD value is higher than the permissible level. The batch cell experiments result worst performance, as the feed concentration increases with time; the polarization is the severest. Hence, for a continuous cross flow mode, the permeate flux as well as qualities are expected to improve. Having established the membrane filtration scheme, i.e., 400 NF followed by RO, the said scheme is then studied in detail in the continuous cross flow systems and are reported in the subsequent section.

Development of ANN model involves training and prediction steps. This batch cell containing flux data (total 216) of nanofiltration (MWCO of 200, 400) and NF followed by RO in our study was

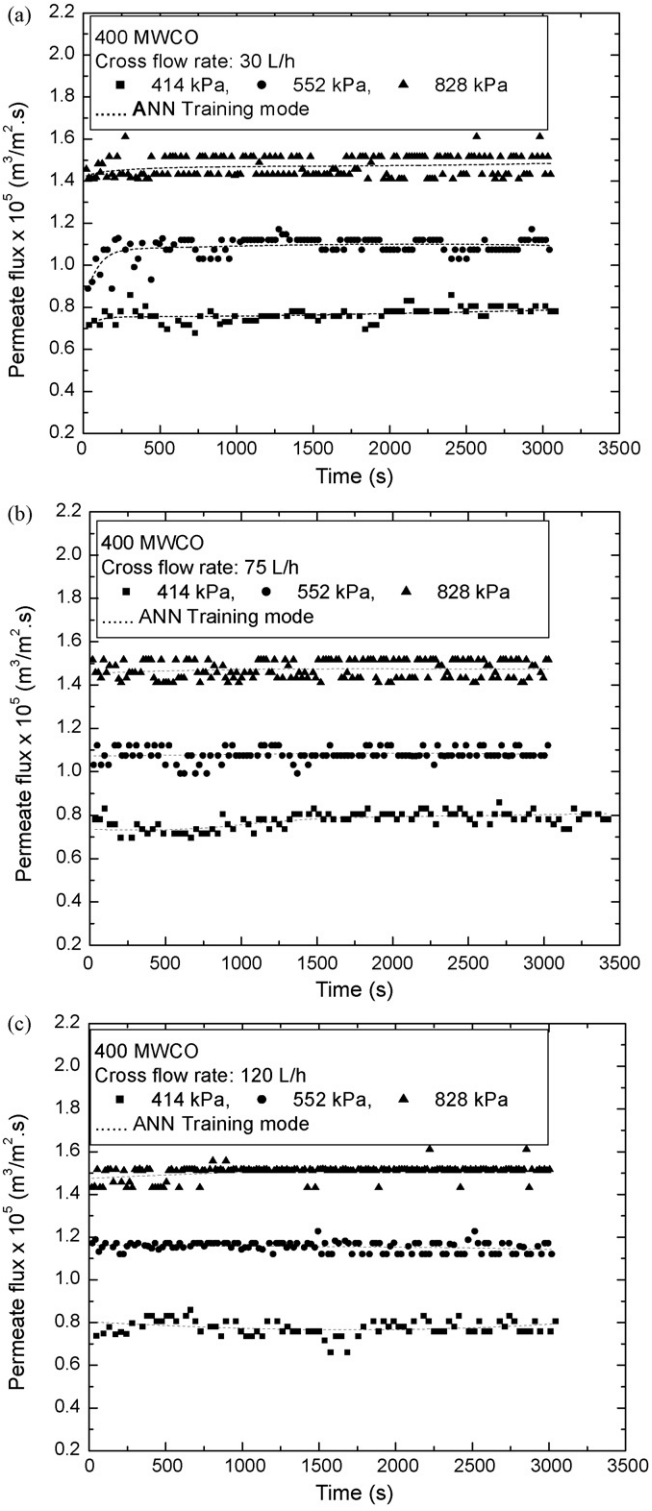

Fig. 6. (a) Experimental permeate flux profiles along with ANN training mode data using 400 MWCO membrane in the cross flow cell under various operating pressures and at a cross flow rate of 30 L/h. (b) Experimental permeate flux profiles along with ANN training mode data using 400 MWCO membrane in the cross flow cell under various operating pressures and at a cross flow rate of 75 L/h. (c) Experimental permeate flux profiles along with ANN training mode data using 400 MWCO membrane in the cross flow cell under various operating pressures and at a cross flow rate of 120 L/h.

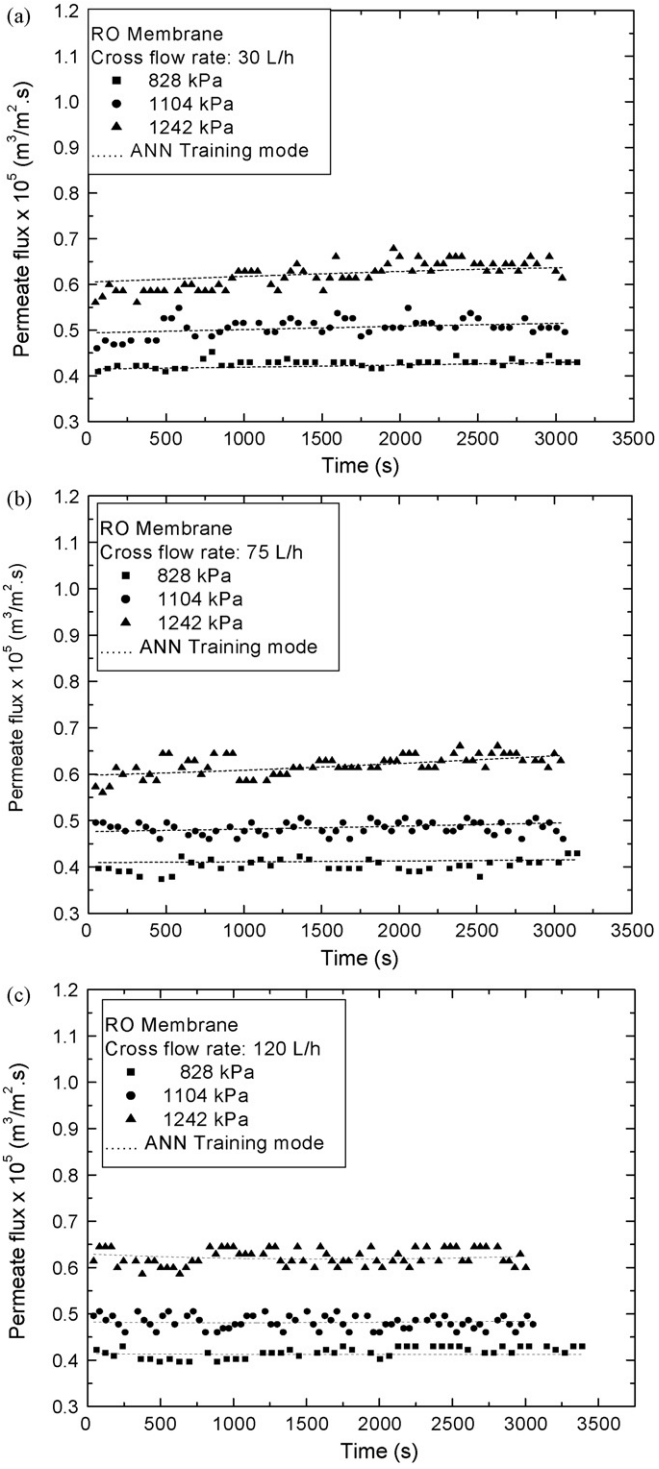

Fig. 7. (a) Experimental permeate flux profiles along with ANN training mode data using RO membrane in the cross flow cell under various operating pressures and at a cross flow rate of 30 L/h. (b) Experimental permeate flux profiles along with ANN training mode data using RO membrane in the cross flow cell under various operating pressures and at a cross flow rate of 75 L/h. (c) Experimental permeate flux profiles along with ANN training mode data using RO membrane in the cross flow cell under various operating pressures and at a cross flow rate of 120 L/h.

Table 7
ANN results for cross flow experimental data.

Sl. No.	Number of neurons	Mean square error ($\times 10^4$)	Number of iterations	Learning rate	Momentum rate
1	3	4.67	190	0.3	0.2
2	4	4.33	180	0.3	0.2
3	(2,1)	2.1	180	0.35	0.25
4	(2,2)	2.40	160	0.35	0.25
5	(3,2)	5.8	170	0.35	0.25
6	(3,3)	2.12	180	0.35	0.25
7	(4,3)	4.26	190	0.35	0.25
8	(4,4)	7.33	210	0.35	0.25
9	(5,4)	4.71	200	0.35	0.25
10	(5,5)	4.15	180	0.35	0.25
11	(6,5)	3.71	230	0.35	0.25

trained with 171 flux data and remaining 45 flux data for prediction. Table 2 explains the experimental conditions and number of data used for training and prediction. Learning rate and momentum rate are varied from 0 to 1. Selection of proper learning factor, momentum factor, number of neurons in hidden layer, and number of iterations influence the training and validation results.

Different configurations of ANN model have been tried and there results are presented in Table 6. It may be observed from Table 6 that the configuration 4-7-1 gives the minimum mean square error (MSE). The training data set responses with different experimental conditions after training are presented in Fig. 4a and b for NF and in Fig. 4c for NF followed by RO data. In the figures, symbols represent the experimental data and the dotted lines represent the results of ANN model. It is clear from the figures that the nature of permeate flux under various experimental conditions is successfully explained by the ANN model. Predicted values are shown in Fig. 5a–c, respectively for 200 MWCO, 400 MWCO and 400 MWCO followed by RO membrane. From figures it is clearly observed that experimental data is closely matching with the results of ANN model.

4.3. Cross flow run

4.3.1. Nanofiltration

Once the concept of the separation in an unstirred batch cell is successfully validated, the effluent is then subjected to a steady state cross flow mode. A detailed parametric study is also conducted to observe the effects of the operating conditions on the permeate flux and permeate quality.

4.3.2. Nanofiltration using 400 MWCO

As stated earlier, the clarified effluent is subjected to 400 MWCO NF (membrane) in the cross flow cell. The variation of the permeate flux with operating time at three different pressure is shown in Fig. 6a–c for the cross flow rates of 30, 75 and 120 L/h, respectively. From figures, it may be observed that the permeate flux increases with pressure as discussed earlier but remains almost constant through out the operating time. For example, with increase of pressure from 414 to 828 kPa, the steady state flux increases from about 0.8×10^{-6} to 1.5×10^{-6} m^3/m^2 s (almost 100% increase). The steady state flux at 120 L/h and 828 kPa is about 1.5×10^{-5} m^3/m^2 s, which is one order of magnitude higher than the batch cell flux at the end of 2 h. From Fig. 6a–c it may be seen that the permeate flux is almost independent of cross flow rate within the experimental range considered herein.

BOD and COD of permeate with pressure is also measured. It is observed that COD increases slowly with pressure due to increase of driving force. For example, at 30 L/h, COD increases from 128 to 142 mg/L as pressure increases from 414 to 828 kPa. The effects of cross flow rate are prominent in this case. At 828 kPa pressure, COD decreases from about 142 to 92 mg/L as flow rate increases

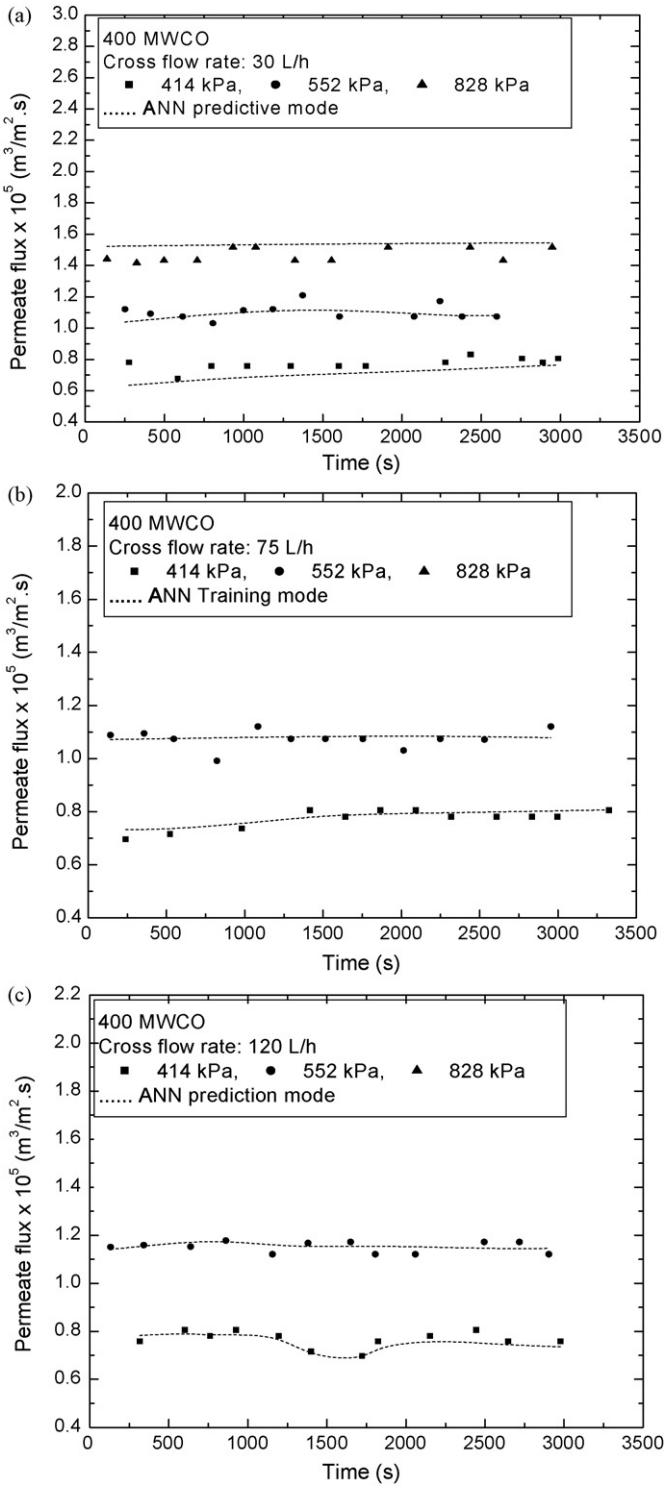

Fig. 8. (a) Experimental permeate flux profiles along with ANN prediction using 400 MWCO membrane in the cross flow cell under various operating pressures and at a cross flow rate of 30 L/h. (b) Experimental permeate flux profiles along with ANN prediction using 400 MWCO membrane in the cross flow cell under various operating pressures and at a cross flow rate of 75 L/h. (c) Experimental permeate flux profiles along with ANN prediction using 400 MWCO membrane in the cross flow cell under various operating pressures and at a cross flow rate of 120 L/h.

30–120 L/h. It may be noted here that permeate COD for all the operating conditions is well within the permissible limit, i.e., below 250 mg/L. The trends of BOD with pressure and flow rate are same as that of COD. But, it is found that apart from the operating conditions (414 kPa and 120 L/h) all BOD values are above 30 mg/L. In fact, the

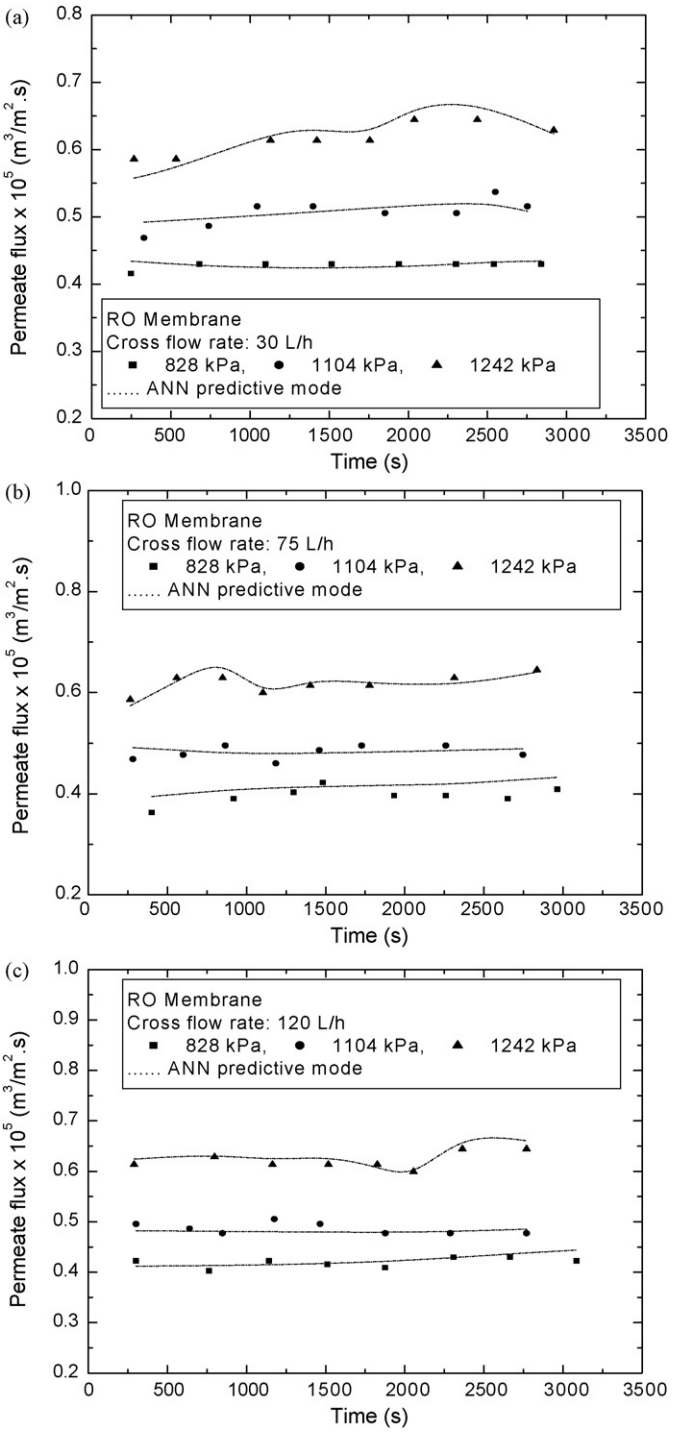

Fig. 9. (a) Experimental permeate flux profiles along with ANN prediction using RO membrane in the cross flow cell under various operating pressures and at a cross flow rate of 30 L/h. (b) Experimental permeate flux profiles along with ANN prediction using RO membrane in the cross flow cell under various operating pressures and at a cross flow rate of 75 L/h. (c) Experimental permeate flux profiles along with ANN prediction using RO membrane in the cross flow cell under various operating pressures and at a cross flow rate of 120 L/h.

lowest BOD is at 30 mg/L, which is the permissible limit. Therefore, although the permeate COD values of NF are within the permissible limit but it is desirable to bring down the BOD below the permissible limit. Therefore, one more filtration step using RO of the permeating solution generated from NF is required.

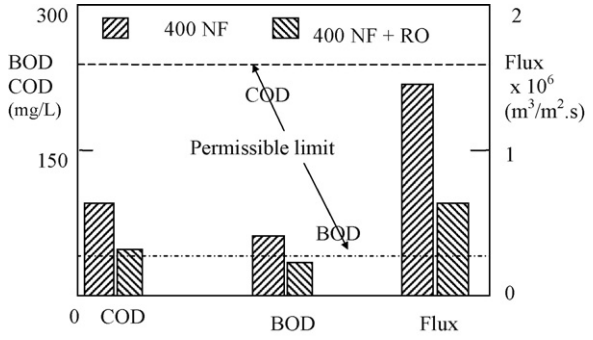

Fig. 10. Comparison of the performance of 400 MWCO NF membrane and 400 MWCO NF membrane followed by RO membrane. Operating pressure, 828 kPa for 400 MWCO NF membrane and 1242 kPa for RO membrane.

4.3.3. NF followed by RO

The variations of the permeate flux with time at three different operating pressures using RO membrane are shown in Fig. 7a–c for various cross flow rates. The steady state flux at 828 kPa and 120 L/h cross flow rate is about 6×10^{-6} m^3/m^2 s, which is almost three times to that of the batch cell data at the end of the operation. The effect of pressure is significant and the steady state flux increases from 4.2 to 6×10^{-6} m^3/m^2 s as the pressure increases from 828 to 1242 kPa. It is also seen from the figures that the cross flow rate considered herein has a marginal effect on permeate flux.

The CODs and BODs are measured at the end of each experiment. It is found that although COD increases slightly with pressure, but all the values are well within the permissible limit. All the BOD values are less than the permissible values except that at the cross flow rate of 30 L/h. The COD and BOD values decrease with the cross flow rate significantly. For example, at 1242 kPa pressure, COD decreases from about 90 to 38 mg/L; whereas, BOD decreases from 40 to 20 mg/L, when the cross flow rate increases from 30 to 120 L/h. Therefore, 1242 kPa pressure and 120 L/h flow rate gives the highest permeate flux and lowest BOD and COD values (well under the specified limits). For NF using 400 MWCO and NF followed by RO, a total number of 1778 experimental data are taken of which 1598 data are used for training purpose and remaining 180 data are used to compare the ANN predicted results. Table 3 explains the experimental conditions and number of data used for training and prediction.

Different configurations of ANN model have been tried and there results are presented in Table 7. Minimum mean square error is observed when 6-5 neurons are in the first and second hidden layers. So from training configuration 4-6-5-1 gives the minimum mean square error (MSE) for the network. The training data with different experimental conditions and the ANN results after training are presented in Fig. 6a–c for NF using 400 MWCO and Fig. 7a–c for NF followed by RO. Similarly ANN prediction data are shown in Fig. 8a–c for NF using 400 MWCO and Fig. 9a–c for NF followed by RO. From Fig. 8a–c and Fig. 9a–c it can be clearly observed that experimental data is closely matching with the results of ANN model for both NF using 400 MWCO and NF followed by RO.

4.4. Comparison of the performance of exclusive NF and NF followed by RO

The comparative performance data of NF using 400 MWCO membrane and NF (400 MWCO) followed by RO is shown in Fig. 10. The operating pressures are 828 kPa and 1242 kPa for NF and RO, respectively. The cross flow rate is 120 L/h. It may be observed from Fig. 10 that COD in both the processes are within the permissible limit. BOD after 400 MWCO NF process is beyond the permissible limit. On the other hand, the permeating solution of RO has a BOD well within the permissible limit. In order to meet the permissible

limit of the treated effluent, one has to sacrifice the permeate flux. From Fig. 10, it is clear that the permeate flux is 1.53×10^{-6} m^3/m^2 s after the NF operation and the flux is about 0.65×10^{-6} m^3/m^2 s after RO. Therefore, the clarified leather effluent may safely be treated using NF followed by RO so that the COD and BOD of the permeate fall safely within the permissible limit and the treated stream can be discharged or reused.

5. Conclusion

In this work, a schematic is proposed to treat the leather plant effluent using membrane separation technique. Experimental investigation is performed to check the validity of the proposed scheme and results are interpreted using ANN technique. All the effluent coming out from various process streams of a leather plant (effluent 1), except chrome tanning, is treated with a series of pretreatment processes, namely gravity settling, coagulation and cloth filtration. The optimum alum dose for coagulation is determined and found to be 1.0 g/L. The supernatant is then subjected to 400 MWCO NF followed by RO membrane. A systematic parametric study is conducted to observe the effects of the operating variables on the permeate flux and quality; both for NF and RO under batch and cross flow mode of operation. A 400 MWCO membrane is found to be more suitable between 200 and 400 MWCO membranes. The suitable operating pressure for NF is 828 kPa and that for RO is 1242 kPa. The cross flow rate 120 L/h is found suitable for both the cases. The permeate BOD and COD of the treated effluent is found to be well within the permissible limit. The possibility of artificial neural network approach is investigated to predict permeate flux for both batch and cross flow run. The optimal model, which consisted of two hidden layer is able to predict permeate flux with mean absolute errors less than 1%. Also the validity of these models has been tested with very good results for unused data at different experimental conditions. Therefore, it is unnecessary to carry out extensive pilot plat testing for collection of data. The developed model will be able to interpolate the process variables at other conditions of interest, with potential great savings in time and cost.

Acknowledgements

The experimental part of the present work is carried out in the membrane separation laboratory of IIT Kharagpur. Many thanks to Prof. S. De and Prof S. DasGupta for giving permission to conduct experiments in their laboratory.

References

[1] J.R. Rao, N.K. Chandrababu, C. Muralidharan, B.U. Nair, P.G. Rao, T. Ramasamy, Recouping the wastewater: a way forward for cleaner leather processing, J. Cleaner Prod. 11 (2003) 591–599.
[2] S.V. More, S. John, B.S. Rao, B.U. Nair, R.S. Laxman, Chromium removal and reduction in COD of tannery effluents by actinomyates, Indian J. Environ. Health 43 (3) (2001) 108–113.
[3] A. Cassano, R. Molinari, M. Romano, E. Drioli, Treatment of aqueous effluents of the leather industry by membrane processes: a review, J. Membr. Sci. 181 (2001) 111–126.
[4] M.T. Ahmed, S. Taha, T. Chaabane, N. BenFare, A. Brahimi, R. Maachi, G. Dorange, Treatment of sulfides in tannery bath by nanofiltration, Desalination 85 (2005) 269–274.
[5] A. Cassano, E. Drioli, R. Molinari, Integration of ultrafiltration into unhairing and degreasing operations, J. Soc. Leather Technol. Chem. 82 (1998) 130–135.
[6] A. Cassano, A. Criscuoli, E. Drioli, R. Molinari, Clean operations in the tanning industry: aqueous degreasing coupled to ultrafiltration: experimental and theoretical analysis, Clean Product Process. 1 (4) (1999) 257–267.
[7] A. Cassano, E. Drioli, R. Molinari, C. Bertolutti, Quality improvement of recycled chromium in the tanning operation by membrane processes, Desalination 108 (1996) 193–203.
[8] W. Scholz, M. Lucas, Techno-economic evaluation of membrane filtration for the recovery and reuse of tanning chemicals, Water Res. 37 (2003) 1859–1867.
[9] A. Cassano, J. Adzet, R. Molirani, M.G. Buonomenna, J. Roig, E. Drioli, Membrane treatment by nanofiltration of exhausted vegetable tanning liquors from the leather industry, Water Res. 37 (10) (2003) 2426–2434.
[10] H.F. Saalan, M.H. Sorour, S.K. Tewfik, Simulation and optimization of a membrane system for chromium recovery from tanning wastes, Desalination 141 (2001) 315–324.
[11] A.P. Padilla, E.L. Tavani, Treatment of an industrial effluent by reverse osmosis, Desalination 126 (1999) 219–226.
[12] A.F. Viero, A.C.R. Mazzarollo, W. Wada, I.C. Tessaro, Removal of hardness and COD from retanning treated effluent by membrane process, Desalination 149 (2002) 145–149.
[13] L.G. Peeva, E. Gibbins, S.S. Luthra, L.S. White, R.P. Stateva, A.G. Livingston, Effect of concentration polarisation and osmotic pressure on flux in organic solvent nanofiltration, J. Membr. Sci. 236 (2004) 121–136.
[14] S. De, S. Bhattachajee, P.K. Bhattacharya, A. Sharma, Generalized integral and similarity solutions for concentration profiles for ultrafiltration, J. Membr. Sci. 130 (1997) 99–121.
[15] S.K. Karode, Unsteady state flux response: a method to determine the nature of the solute and gel layer in membrane filtration, J. Membr. Sci. 188 (2001) 9–20.
[16] S. De, P.K. Bhattacharya, Modeling of ultrafiltration process for a two component aqueous solution of low and high (gel-forming) molecular weight solutes, J. Membr. Sci. 136 (1997) 57–69.
[17] J. Hermia, Constant pressure blocking filtration laws—application to power law non-Newtonian fluids, Trans. Chem. Eng. Res. Des. 60a (1982) 183–187.
[18] S. Kosinstev, R.G. Holdich, I.W. Cumming, V.M. Starov, Modeling of dead end microfiltration with pore blocking and cake formation, J. Membr. Sci. 208 (2002) 181–192.
[19] C. Ho, A.L. Zydney, A combined pore blocking and cake filtration model for protein fouling during microfiltration, J. Colloid Interface Sci. 232 (2000) 389–399.
[20] S.T. Kelley, A.L. Zydney, Mechanism for BSA fouling during microfiltration, J. Membr. Sci. 107 (1995) 115–127.
[21] G. Jonsson, P. Pradanos, A. Hernandez, Fouling phenomena in microporous membranes. Flux decline kinetics and structural modifications, J. Membr. Sci. 112 (1996) 171–183.
[22] W.R. Bowen, J.I. Calvo, A. Hernandez, Steps of membrane blocking in flux decline during protein microfiltration, J. Membr. Sci. 101 (1995) 153–165.
[23] M. Mondor, B. Girard, C. Moresoli, Modeling of flux behavior for membrane filtration of apple juice, Food Res. Int. 33 (7) (2000) 539–548.
[24] P. Blanpain, M. Lalude, Investigation of fouling mechanisms governing permeate flux in the cross flow microfiltration of beer, Filtration Sep. 34 (10) (1997) 1065–1069.
[25] L. Huang, M.T. Morrissey, Fouling of membranes during microfiltration of surimi wash water: roles of pore blocking and surface cake formation, J. Membr. Sci. 144 (1998) 113–123.
[26] J.A. Suarez, J.M. Veza, Dead end microfiltration as advanced treatment for wastewater, Desalination 127 (2000) 47–58.
[27] W. Yuan, A. Kocic, A.L. Zydney, Analysis of humic acid fouling during microfiltration using a pore blockage-cake filtration model, J. Membr. Sci. 198 (2002) 51–62.
[28] M.K. Purkait, S. DasGupta, S. De, Resistance in series model for miceller enhanced ultrafiltration of eosin dye, J. Colloid Interface Sci. 270 (2004) 496–506.
[29] P. Aimar, C. Taddei, J.P. Lafaille, V. Sanchez, Mass transfer limitations during ultrafiltration of cheese whey with inorganic membranes, J. Membr. Sci. 38 (1998) 203–221.
[30] M.B. Menhaj, Fundamentals of Neural Networks, Professor Hesabi Publications, Tehran, 1998.
[31] I. Bardot, L. Bouchereau, N. Martin, B. Alagos, Sensory instrumental correlation by combining data analysis and neural network techniques, Food Qual. Pref. 51 (2) (1994) 159–166.
[32] M.C. Bishop, Neural network and their applications, Rev. Sci. Instrum. 64 (1994) 1803–1831.
[33] T. Masters, Practical Neural Network Recipes in C++, Academic Press, London, 1993.
[34] M.K. Purkait, S. DasGupta, S. De, Resistance in series model for micellar enhanced ultrafiltration of eosin dye, J. Colloid Interface Sci. 270 (2004) 496–506.
[35] M.K. Purkait, S. DasGupta, S. De, Separation of aromatic alcohols using micellar enhanced ultrafiltration and recovery of surfactant, J. Membr. Sci. 250 (2005) 47–59.
[36] American Public Health Association, Standard Methods for Examination of Water and Waste Waters, 16th ed., APHA, Washington DC, 1985.
[37] V.K. Jindal, V. Chauhan, Neural networks approach to modeling food processing operations, in: J. Irudayaraj (Ed.), Food Processing Operations Modeling: Design and Analysis, Marcel Dekker, Inc., New York, 2001.
[38] C.K. Mohan, K. Mehrotra, S. Ranka, Elements of Artificial Neural Network, MIT Press, 1997.
[39] P. Danilo, J.A. Chambers, Recurrent Neural Networks for Prediction: Learning Algorithms, Architectures and Stability, John Wiley and Sons, 2001.